# Field Observations and Preliminary Investigations of a Wave Event in Solid Drift Ice in the Barents Sea

Aleksey Marchenko[1], Jean Rabault[2], Graigory Sutherland[2], Clarence O. Collins III[3],
Peter Wadhams[4], Mikhail Chumakov[5]
[1] The University Centre in Svalbard, Longyearbyen, Norway
[2] University of Oslo, Oslo, Norway
[3] Naval Research Laboratory, Stennis Space Center, Hancock County, Mississippi, USA
[4] Univetrsity of Cambridge, Cambridge, UK
[5] Gazprom VNIIGAZ LLC, Moscow, Russia

## ABSTRACT

Waves propagating below drift ice were observed in the North-West Barents Sea. In-situ measurements of ice and water characteristics were performed with the equipment deployed on the ice and in the water below the ice during 16 hours from 16:00, May 1, to 08:00, May 2, 2016. Peak frequencies of the observed waves were around 0.35 rad/s, 0.5 rad/s, 0.6 rad/s and 0.8 rad/s. It is found that the eddy viscosity in the boundary layer below the ice has a mean value of 140 cm$^2$/s with significant variations correlated with the floe acceleration. Spectral properties of the observed waves are compared with the results of the WaveWatch III model. The origin of the observed waves is discussed in the paper.

KEY WORDS: waves, ice, turbulence, drift

## INTRODUCTION

Propagation of wind waves and swell in ice covered regions can influence the break up of drift ice into small floes in a span of a few hours over relatively large areas. At the same time, drift ice influences damping of surface waves and prevents their propagation over long distances in ice covered regions. In regions of offshore activities, broken ice and icebergs accelerated by waves create risks to human activities. Investigation of wave interaction with ice is of interest for the development of human activity in the Barents Sea. There are regions where the water is consistently covered by solid drift ice in the winter time and other regions which are exposed to stronger wave action with rare occurrences of drift ice. Collins et al (2015) described details of ice break up in the Barents Sea due to the penetration of storm waves from open waters.

An analysis of some previous in-situ measurements of wave characteristics in ice covered regions of the Barents Sea is presented by Marchenko et al, 2015. Measurements were performed with an Acoustic Doppler Velocimeter (ADV, SonTek 5MHz Ocean Probe)
POAC17-087

deployed on the drift ice in a downward looking position and a Directional Waverider buoy deployed on top of the ice. Typical periods of waves observed below the drift ice were 10-12 s. The results of ADV measurements gave the possibility to calculate the eddy viscosity in the under-ice boundary layer. According to Liu and Mollo-Christensen (1988) the eddy viscosity influences wave damping. Field measurements have shown great variability of the eddy viscosity from very small values of about 0.002 cm$^2$/s to 100 cm$^2$/s (Marchenko et al, 2015). The high values of the eddy viscosity were found from the analysis of field data collected near Edgeøya. The increase of the eddy viscosity is explained by the influence of non-stationary ice drift on the surface water layer. Representative damping distance for a swell with period of ten seconds is 10-20 km when the eddy viscosity is about 100 cm$^2$/s. Wind waves with periods of 5-6 s dampen over shorter distance and, therefore, were never observed in solid ice.

Previously, Marchenko et al (2013) introduced a method for wave measurement from the ice with two pressure recorders SBE-39 mounted on the same wire at different depths. The method was used to register waves propagating from the front of Tuna glacier due to calving events. Rabault et al (2016) constructed instruments based on Inertial Motion Units (IMUs) and used them for the registration of surface waves penetrating below the ice from the open water in Templefjorden in Spitsbergen. The IMUs were configured to output acceleration and angular rate at 10Hz. In May 2016 all sensors previously cited, including the ADV, SBE-39 and 10 IMUs were deployed on the drift ice near Edgeøya and registered wave characteristics synchronously during 16 hours. In the present paper we described and analyze the results of those field measurements, and compare the output from the different processing methods.


**LOCATION AND ORGANIZATION OF THE FIELDWORK**

Fieldwork was performed on the drift ice near Edgeøya in the North-West Barents Sea (Figure 1a). The geographical coordinates are 77.76$^o$N, 25.5$^o$E. Sea depth in the region was measured around 160 m. RV Lance was moored to a floe of thickness around 30 cm and diameter around 2 km (Figure 1b). The floe mass is estimated between $7 \cdot 10^5$ tons and $8 \cdot 10^5$ tons. The mass of the fully loaded Lance is $M_L$=2370 tons, and her length and breadth are around $L_L$=60m and $w_L$=12 m. Therefore the influence of the Lance on the floe dynamics is small. The frequency of natural oscillations of the Lance is estimated from the formula $\omega_L{}^2 = \rho_w g S_L/M_L$, where $\rho_w$ is the water density, $g$ is the gravity acceleration, and $S_L = w_L L_L$. We find a natural frequency of $\omega_L \approx 1.7$ rad/s, i.e. a period $T_L \approx 3.5$ sec. This is outside of the range of wave frequencies, and therefore cannot be mistaken for incoming water waves.

The equipment was deployed on the floe in the afternoon of May 01, 2016, and wave measurements started from 16:00, May 01 (here and further UTC is used), and extended until 09:00, May 02. The equipment consists of the pressure and temperature recorders SBE 39, Acoustic Doppler Velocimeter SonTek Ocean Probe 5 MHz (ADV), Ice tracker Oceanetic Measurement (model 703 equipped with anemometer) and Inertial Motion Units (IMUs) from Vectornav (VN100). SBE 39 were fixed on a steel wire on the depths 3.6 m and 11.4 m, and the wire was mounted on the ice (Figure 2a). The ADV probe is equipped with tiltmeter and compass. Magnetic inclination is about 15$^o$ in the region and is taken into account during data processing. The ADV was mounted on a vertical wooden pole fixed on the ice with a

tripod (Figure 2a). Velocity measurements were performed at a depth of 80 cm below the ice. The depth is measured by the ADV pressure sensor. SBEs were deployed around 16:00, May 01, and recovered around 09:00, May 02. The ADV sensor was deployed on 19:00, May 01, and around 04:30, May 02, it was disconnected from the electric power source on the Lance board because of the floe motion relatively the ship. The ice tracker was deployed on the floe around 11:00 and sent data via Iridium during one month. The positions of the 10 IMUs deployed are presented in Figure 2b. One IMU was deployed alone, while all other IMUs were grouped into arrays of three sensors.



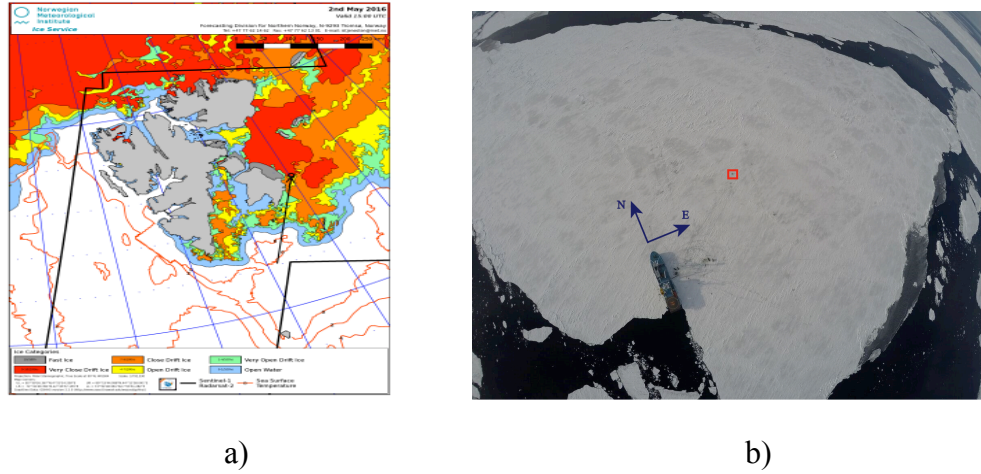a)                                                              b)

Figure 1. (a) Location of the field works near Edgeøya on May 1-2, 2016, is shown on the ice map by black circle and arrow. (b) View of RV Lance from unmanned helicopter. Red square shows location of ADV and SBE
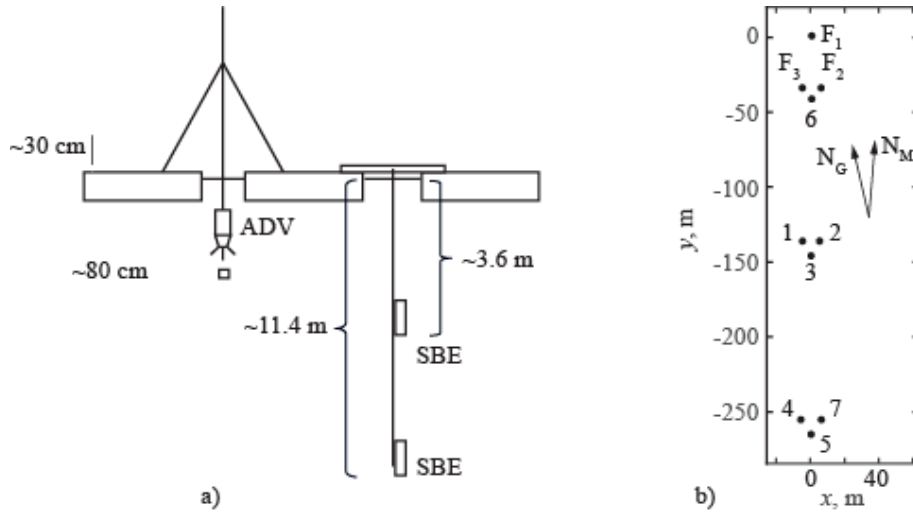


a)                                                              b)

Figure 2. (a) Schematic of the deployment of ADV and SBE sensors. (b) Positions of the IMUs on the ice floe. $N_M$ and $N_G$ indicate the position of the Magnetic and Geographic North, respectively.

User setup for the ADV measurements is given in Table 1. SBE sensors provided continue record with sampling frequency 2 Hz. Ice tracker provided data on GPS location of the

tracker, its yaw angle and local wind velocity with sampling period of 10 min. The trajectory and the drift velocity of the ice tracker are shown in Figure. Wind velocity (Figure 3a) didn't change significantly 16:00 UTC, May 01, to 04:00 UTC, May 02. The shape of the floe trajectory (Figure 3a) and the evolution with time of the flow velocity are explained by the influence of sea current modulated by semidiurnal tide. Evolution of the floe acceleration and yaw angle shown in Figure 4 are explained by the floe interaction with surrounding ice.

Table 1. User setups of ADV.

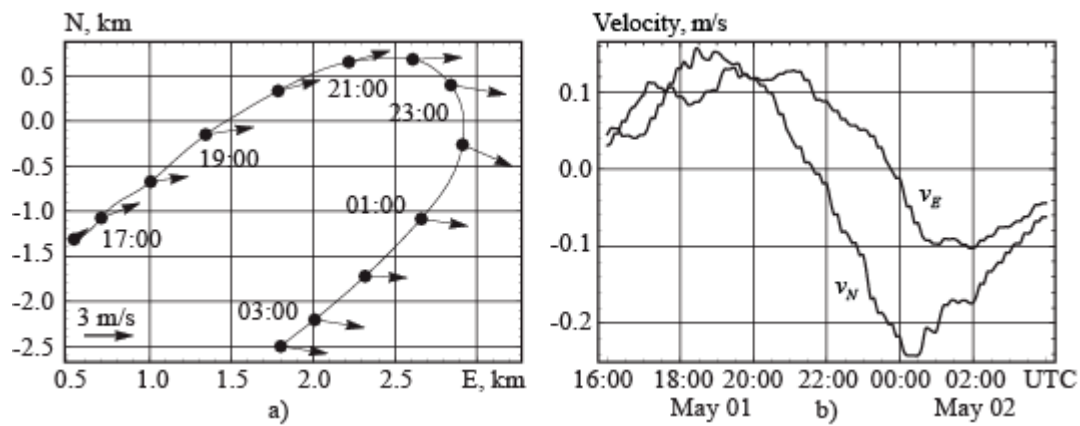| Sensor | Sampling frequency, Hz | Burst Interval, s | Samples per burst | Number of bursts | Depth, cm |
|--------|------------------------|-------------------|-------------------|------------------|-----------|
| ADV | 10 | 360 | 2400 | 94 | 80 |



Figure 3. Trajectory (a) and drift velocity components versus the time (b) of the ice tracker deployed on the ice floe.    Vectors of the wind velocity measured along the drift trajectory are shown by arrows (a).
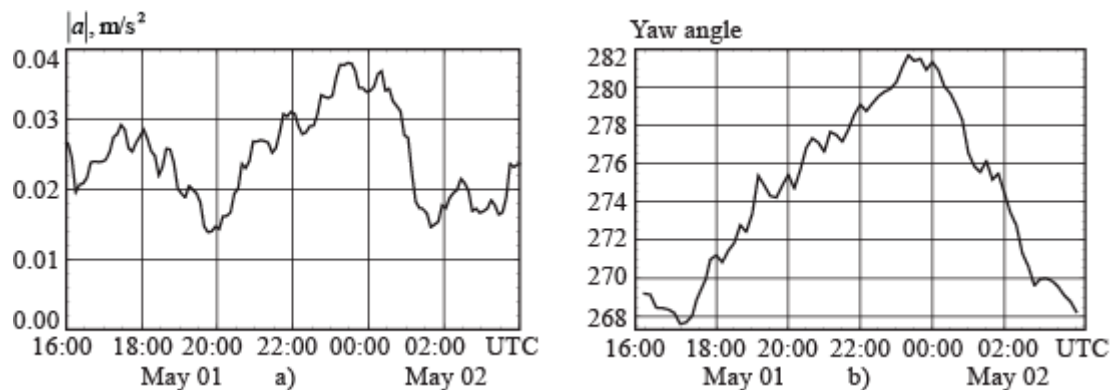


Figure 4. Absolute value of the acceleration (a) and yaw angle (b) of ice tracker deployed on the drift floe versus time.

## ANALYSIS OF SBE DATA

Records of the water pressure measured by both SBE39s are shown in Figure 5. The quality of the data recorded at 3.6 m depth before 21:00 is not sufficient to distinguish wave induced oscillations of the water pressure, but after 21:00 the oscillations are well visible (Figure 5a). The oscillations are well visible in the pressure data recorded at 11.4 m depth from 16:00. Spectral analysis was performed with pressure fluctuations $\delta p$ calculated as a difference between the pressure averaged over each consequent 5 min interval and actual pressure measured in this interval. Spectrograms (Figure 6a) and spectrums (Figure 7) constructed in Mathematica software show that wave spectrum has four local maxima at frequencies around 0.35 rad/s, 0.5 rad/s, 0.6 rad/s and 0.8 rad/s before 23:00, May 01, and there are only two local maxima at frequencies around 0.35 rad/s and 0.6 rad/s after 00:00, May 02. The frequency of waves with maximal energy was 0.8 rad/s before 23:00, May 01, and 0.6 rad/s after 00:00, May 02. Spectrums of the pressure fluctuations recorded at 3.6 m depth are very similar to shown in Figure 7.
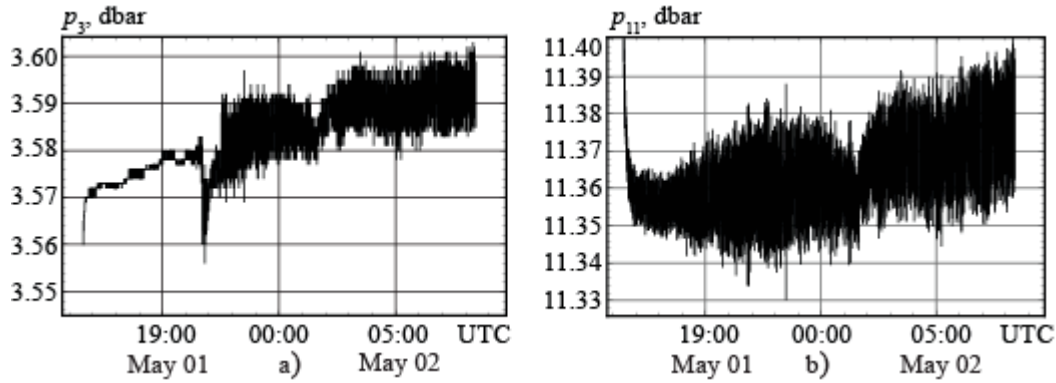


Figure 5. Records of the water pressure measured by recorders SBE39 deployed at 3.6 m (a) and 11.4 m (b) depths.

It was shown (Marchenko et al, 2013) that the ratio of wave induced pressure amplitudes measured at depths $z=z_1$ and $z=z_2$ is equal to:

$$\gamma \equiv \frac{p_{1,dyn}}{p_{2,dyn}} = \frac{\omega^2 \cosh[k(z_1+H)] - gk \sinh[kH]}{\omega^2 \cosh[k(z_2+H)] - gk \sinh[kH]}. \tag{1}$$

Eqn. (1) is used for the calculation of the wave number $k$ when the wave frequency is known. We consider the Fourier transforms $\delta p_{3,f}(\omega)$ and $\delta p_{11,f}(\omega)$ of the pressure fluctuations $\delta p_3(t)$ and $\delta p_{11}(t)$ recorded at depths 3.6 m and 11.4 m. It is assumed that the ratio $\gamma$ is equal to the ratio $|\delta p_{3,f}|/|\delta p_{11,f}|$, where the values of $|\delta p_{3,f}|$ and $|\delta p_{11,f}|$ are taken in the points of their local maxima shown in Figure 6 by grey and black circles. The values of $|\delta p_{3,f}|$ and $|\delta p_{11,f}|$ in their local maxima are given in Table 2. Black dots in Figure 8a have coordinates $(k, \omega)$, where the values of $\omega$ are taken from Table 2, and the values of $k$ are calculated from Equn. (1) with the values of $\omega$ and $\gamma$ calculated using Table 2. Solid line in Figure 8a shows the dispersion relation of gravity waves propagating in the water with free surface and described by the
POAC17-087

formula $\omega^2=gk\cdot\tanh(kH)$ with $H$=160 m. One can see that experimental points sit on the dispersion curve. It means that the influence of ice on dispersion properties of observed waves is very small.

The last conclusion follows from the dispersion equation of flexural-gravity waves $\omega^2=gk\cdot\tanh(kH)(1+Dk^4)$, when $Dk^4\ll1$. Here $D\approx Eh^3/(12\rho_w g)$, where $E$ is the effective elastic modulus of the ice and $h$ is the ice thickness. In-situ tests of flexural strength of floating cantilever beams performed on the drift ice on May 01 shown that $E$=1.2-1.9 GPa. Assuming $h$=0.3 m we find that $Dk^4<0.01$ when $k$=0.07, i.e. the influence of ice elasticity on the waves with registered frequencies is expected to be very small, in good agreement with observations.

Wave amplitude is calculated using water pressure records at depth $z$ below the ice and the formulae:

$$\delta p_{z,f}(\omega)=\rho_w g\eta_f(\omega)P(k,z),\quad P(k,z)=\frac{\cosh[k(z+H)]}{\cosh[kH]}-1, \tag{2}$$

where $\delta p_{z,f}$ and $\eta_f$ are the Fourier images of the water pressure fluctuations $\delta p_z(t)$ at the depth $z$ and water surface elevation $\eta(t)$ caused by waves. We used records of the water pressure at 11 m depth. Values of $\delta p_{z,f}$ were calculated using the discrete Fourier transform in Mathematica. Then the inverse Fourier transform was used to calculate water surface elevation as a function of the time separately. The procedure was realized independently for each hour of the record. Significant wave height ($SWH$) is calculated using the formula:

$$SWH=4\cdot\mathrm{StandardDeviation}[\eta]. \tag{3}$$

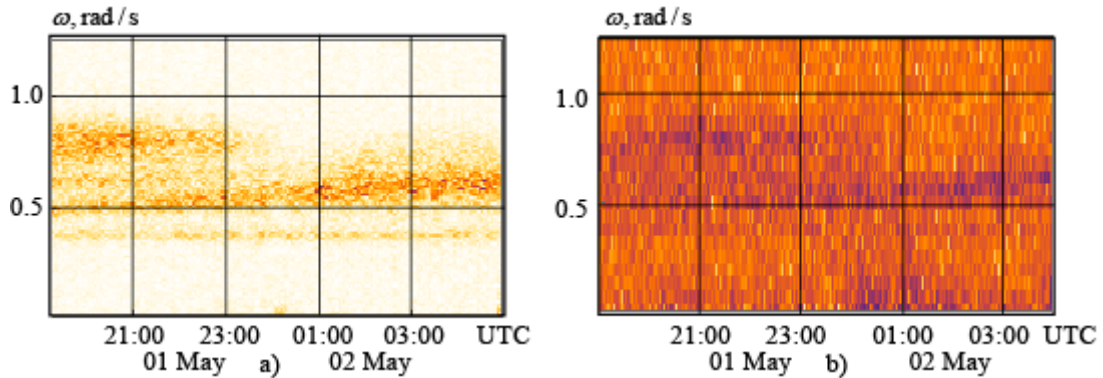Mean value of SWH was found around 10 cm.



Figure 6. Spectrogram of pressure fluctuations reconstructed with SBE data recorded at 11.4 m depth (a). Spectrogram of the fluctuations of the North component of water velocity recorded by ADV (b).
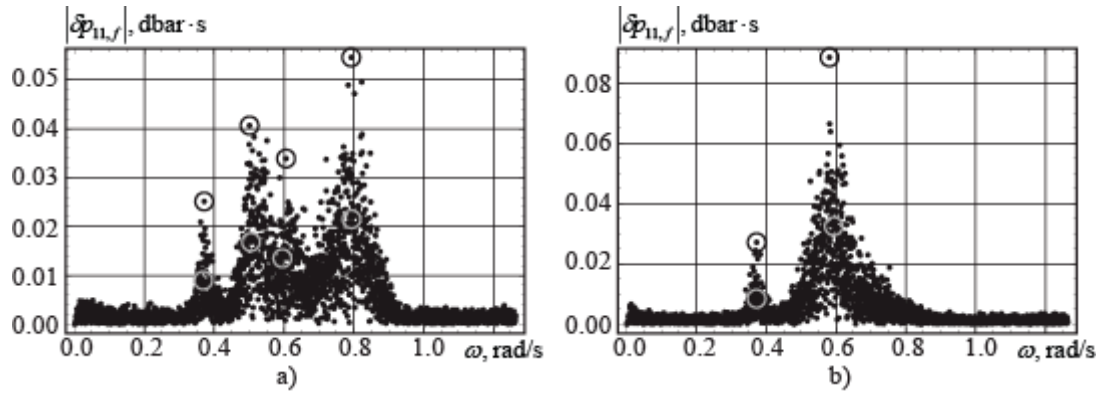
Figure 7. Spectra of water pressure fluctuations recorded at 11.4 m depth from 19:00 to 23:00, May 01, (a) and from 23:00, May 01, to 03:00, May 02, (b). Black and gray circles show spectral maxima of pressure fluctuations records at 11.4 m and 3.6 m depths.

Table 2. Local maxima of spectrums $|\delta p_{3,f}|$ and $|\delta p_{11,f}|$, dbar·s.

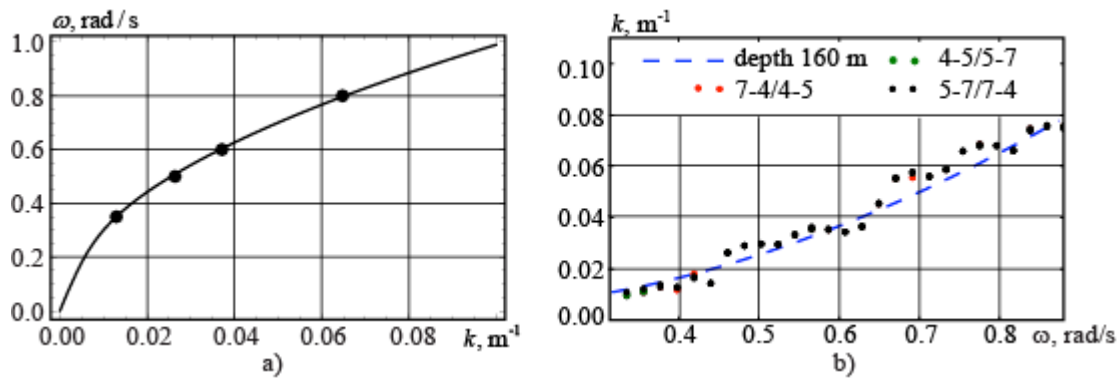| | 19:00 to 23:00, May 01 | | | | 23:00, May 01, to 03:00, May 02 | |
|---|---|---|---|---|---|---|
| $\omega$, rad/s | 0.35 | 0.5 | 0.6 | 0.8 | 0.35 | 0.6 |
| 3.6 m | 0.009 | 0.017 | 0.013 | 0.021 | 0.009 | 0.032 |
| 11.4 m | 0.026 | 0.04 | 0.034 | 0.054 | 0.025 | 0.09 |



Figure 8. Dispersion relation of surface gravity waves in the water of 160 m depth. Black dots are constructed using SBE records at 3.6 m and 11.4 m depths (a). Dispersion relation obtained from the analysis of the cross correlation between IMU signals 4, 5 and 7 using Eqn. (11), at 20:00 UTC on 01/05/2016 (b).

**ANALYSIS OF ADV DATA**

Records of the East ($v_E$) and North ($v_N$) velocity components at 80 cm depth below the ice were used for the calculation of the eddy viscosity and the analysis of spectrums and directions of wave propagation. The velocity fluctuations in the East ($\delta v_E$) and North ($\delta v_N$)

POAC17-087

directions were calculated for each burst of the ADV record as follows:

$$\delta v_E = v_E - \langle v_E \rangle, \quad \delta v_N = v_N - \langle v_N \rangle, \tag{4}$$

where $\langle v_E \rangle$ and $\langle v_N \rangle$ are the mean values of the East and North velocities averaged over the burst. All fluctuations were grouped in one file and used for the construction of spectrogram. The spectrogram of the fluctuations of the North velocity component is shown in Figure 6b. It looks similar to the spectrogram constructed with the SBE data. Spectrums of $\delta v_N$ are shown in Figure 9. Spectral maxima are well visible in the spectrums of $\delta v_N$ and are absent in the spectrum of $\delta v_E$ from 19:00 to 23:00, May 01. The $\delta v_N$ spectrum looks very similar to the spectrum shown in Figure 7a. Figure 9b shows spectral maxima at the frequency of 0.6 rad/s in the spectrum $\delta v_N$. There is spectral maxima in the spectrum of $\delta v_E$ at the same frequency. Spectral maxima at the frequency of 0.35 rad/s appears only in the spectrum of $\delta v_N$. The velocity directions should be corrected by clockwise shift on $15^{\circ}$ because of the magnetic inclination.
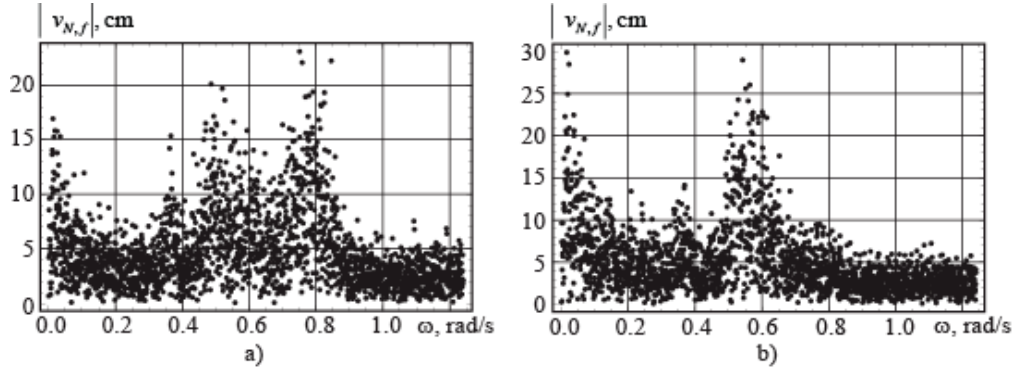


Figure 9. Spectrums of fluctuations of the North velocity component recorded from 19:00 to 23:00, May 01, (a) and from 23:00, May 01, to 03:00, May 02, (c).
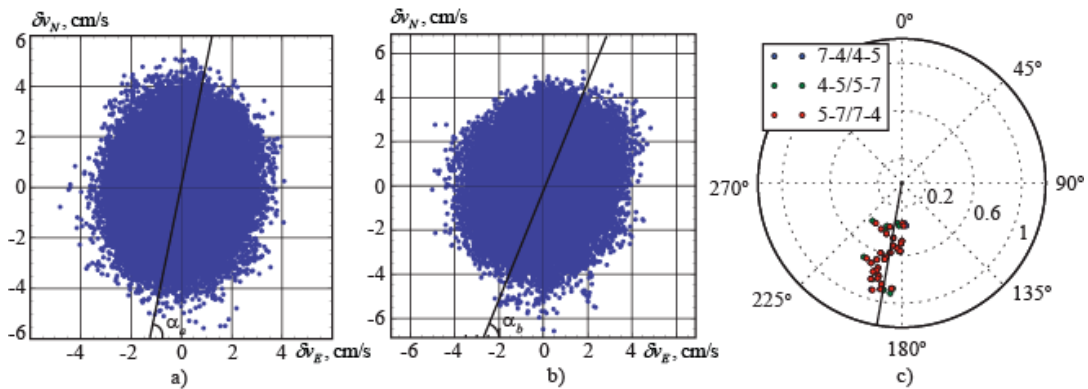


Figure 10. Hodograph of the velocity fluctuations recorded from 19:00 to 23:00, May 01, (a) and from 23:00, May 01, to 03:00, May 02, (b). (c): direction of propagation of the waves obtained from the analysis of the cross correlation between IMU signals 4, 5 and 7 using Eqn. (11), at 20:00 UTC on 01/05/2016, concentric circles indicate wave frequency rad/s). The black line indicates the direction of azimuth 190 degrees.

POAC17-087

Each point in Figure 10a,b corresponds to the vector of the velocity fluctuations with corrected direction. The sampling frequency is 10 Hz. From Figure 10a it follows that dominant direction of wave propagation from 19:00 to 23:00, May 01, was from the South-West with azimuth angle $\alpha_a \approx 189.6^o$. Later from 23:00, May 01, to 03:00, May 02, the azimuth angle of wave propagation increased to $\alpha_b \approx 199.8^o$ (Figure 10b).
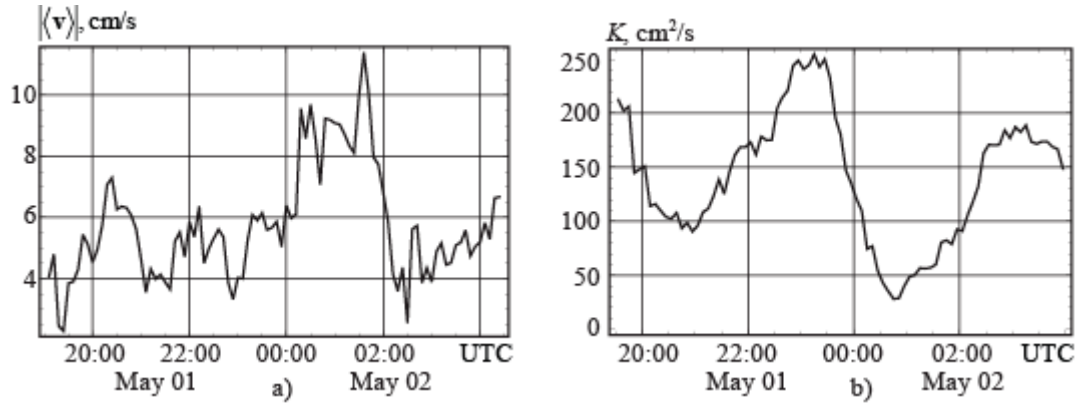


Figure 11. The mean horizontal water velocity relatively the ice (a) and the eddy viscosity (b) versus the time.

Figure 11a shows the mean horizontal velocity of the water below the ice measured with the ADV versus the time. Figure 11b shows the eddy viscosity versus the time. The eddy viscosity is calculated with the formula:

$$\tau = -\rho_w K \frac{\partial \langle v_h \rangle}{\partial z},$$ (5)

where $\tau$ is the turbulent shear stress applied to the ice at the ice-water interface, $\rho_w$ is the water density, $\langle v_h \rangle$ is the mean horizontal velocity of the water relative to the ice, $z$ is the vertical coordinate, and $K$ is the eddy viscosity.

The turbulent shear stresses applied to the ice bottom in the East and North directions are calculated with the formula of Reynolds stresses:

$$\tau_E = \rho_w \langle \delta v_E \delta w \rangle, \quad \tau_N = \rho_w \langle \delta v_N \delta w \rangle,$$ (6)

where $\delta w$ is the fluctuation of the vertical velocity, and symbol $\langle .. \rangle$ means the averaging over the burst. The turbulent shear stress $\tau$ in Eqn. (4) is calculated from the formula:

$$\tau = \sqrt{\tau_E^2 + \tau_N^2}.$$ (7)

The vertical gradient of the mean horizontal velocity of the water relatively the ice is approximated as $\partial \langle v_h \rangle / \partial z \approx -\langle v_h \rangle / h_{ADV}$, where $h_{ADV} = 80$ cm. The mean horizontal velocity is

calculated from the formula:

$$\langle v_h \rangle = \sqrt{\langle v_E \rangle^2 + \langle v_N \rangle^2} \ . \tag{8}$$

From Figure 10 it follows that $K$ reaches a local maximum in time when $\langle v_h \rangle$ is minimal, and when the floe acceleration shown in Figure 3a. The mean value of the eddy viscosity over is found to be $140 \text{cm}^2/\text{s}$.

**ANALYSIS OF IMU DATA**

The signals recorded by the IMUs are of good quality, as confirmed by the example of raw data shown in Figure 12. The PSD of the wave elevation is computed from the PSD of the wave vertical acceleration following the formula: $PSD[\eta] = \omega^{-4} PSD[\eta_{tt}]$, where $\eta$ is the wave elevation. Excellent agreement is found between the shape of the PSD reported in Figure 7a and the one reported in Figure 12 (right), which validates both methods. Significant wave height can be obtained from the zeroth order moment of the PSD, and the results are very similar to what is obtained from Eqn. (3), with a maximum value of around 12 cm.
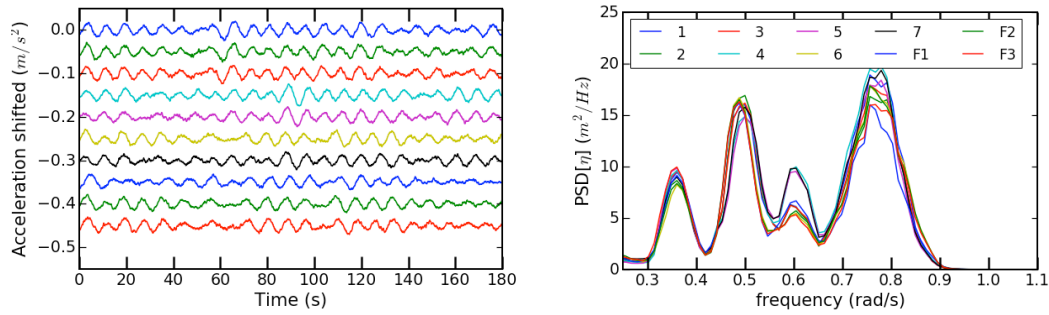


Figure 12. Left: sample of the raw signal for vertical acceleration recorded by all 10 IMUs starting at UTC time 20:00:00.000 on 01/05/2016 (vertical offsets are used for ease of visualization). Right: PSD of wave elevation computed for the 10 IMUs at the same time as presented in Figure 7 (a), using Welch method on 30 minutes intervals with 75% overlap.

The signals obtained by each set of 3 sensors grouped together can be used to perform a 2D cross-correlation analysis, extending what was presented by Sutherland and Rabault (2016). The normalized cross-spectral density is computed between adjacent sensors as:

$$C_{xy} = \frac{|S_{xy}|^2}{S_{xx}S_{yy}}, \text{ with } S_{xy}(f) = \frac{1}{2\pi} \sum_{n=-N/2}^{n=N/2} R_{yx}(n)e^{-j2\pi fn} \ , \tag{9}$$

where $R_{xy}(n)$ is the cross-correlation between the discrete signals $x(n)$ and $y(n)$. The phase shift of the waves between two adjacent sensors is then computed at all frequencies for which the coherence is significant with a probability higher or equal to 95%, following the formula:

$$\phi_{xy}(f) = \arctan 2 \left( \frac{\text{Im}[S_{yx}(f)]}{\text{Re}[S_{yx}(f)]} \right) \qquad (10)$$

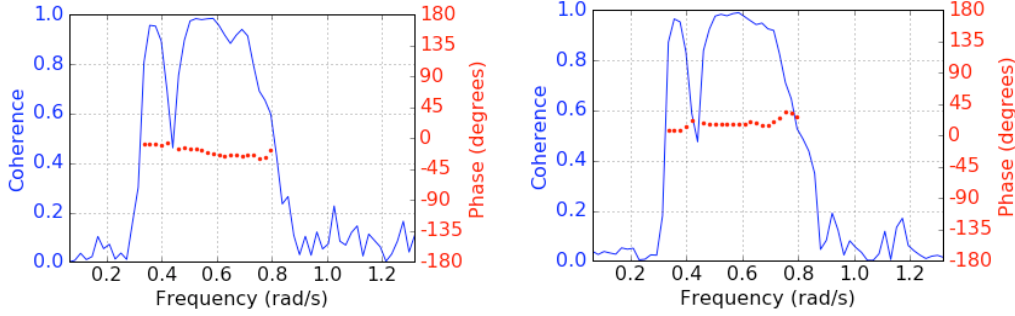Typical outputs from this method are presented in Figure 13.



Figure 13: coherence and phase shift of the wave acceleration recorded between sensors F2 and F3 (left) and F3 and 6 (right). Coherence is computed based on a 45 minute interval, with 75 percent overlap between segments.

The phase shift between adjacent sensors is related to the incoming waves through the relation: $\phi_{ij}(f) = \vec{k}(f) \cdot \vec{x}_{if}$ (Eqn. 11), where $\vec{k}(f)$ is the incoming wave vector at frequency f and $\vec{x}_{ij}$ is the vector from IMU i to IMU j. Therefore, the two dimensional wave vector can be obtained at each frequency using the phase shift from two sides of a triangle of sensors and elementary trigonometry. This gives access to both the direction of the incoming waves and the dispersion relation. An example of the results of such analysis is presented in Figure 8b and Figure 10c. Similar to what is presented in Figure 8a,b, the waves are found to follow the deep water dispersion relation and the effect of the ice is negligible. The direction of propagation of the waves is also in very good agreement with the results presented in Figure 10a.

**COMPARISON WITH NUMERICAL SIMULATIONS**

Wave frequency and wave direction of propagation were obtained from the web (https://earth.nullschool.net), where the results of modeling with WaveWatch III are provided. Figure 14 shows that there are two wave systems coming to Spitsbergen from South-West and from South-East. The white line in Figure 14 marks the boundary between them. Waves coming from the South-West have periods around 10 sec, and waves coming from the South-East have periods around 6.3 sec near Spitsbergen. According to WaveWatch III, the dominant wave period and direction of propagation at the point (76.93 N, 21.60 E) is shown in Figure 14 by a white circle were 8.4 s and 210° on 22:00, May 01, and 10.1 s and 205° on 02:00, May 2. Frequencies of waves in the region extended to the East from the marked location are around 5-6 sec. Spectra in Figure 7 show the dominant wave frequency to be 0.8 rad/s (wave period 7.8 sec) before 23:00, May 01, and 0.6 rad/s (wave period 10.4 s) after 23:00, May 01. Thus the waves observed propagate from the South-West along the shore of

Edgeøya. The ice map in Figure 1a shows green and yellow regions of very open drift ice which extended along Edgeøya. The waves arrive at the observation site following this route.

## CONCLUSIONS

In-situ records of water and ice characteristics are performed on the drift floe in the North-West Barents Sea during wave propagation event of 16 hours duration. The ice floe of 30 cm thickness was cyclically bended by waves with an amplitude of several centimeters and was not broken. Spectral analysis has shown the existence of local spectral maxima at the frequencies 0.35 rad/s, 0.5 rad/s, 0.6 rad/s and 0.8 rad/s. Dominant waves with frequencies 0.6 rad/s and 0.8 rad/s propagated from South-West along the Edgeøya shoreline. Several measurement methods are presented and validated against each other, including direct measurement of the dispersion relation and of the direction of propagation of waves.
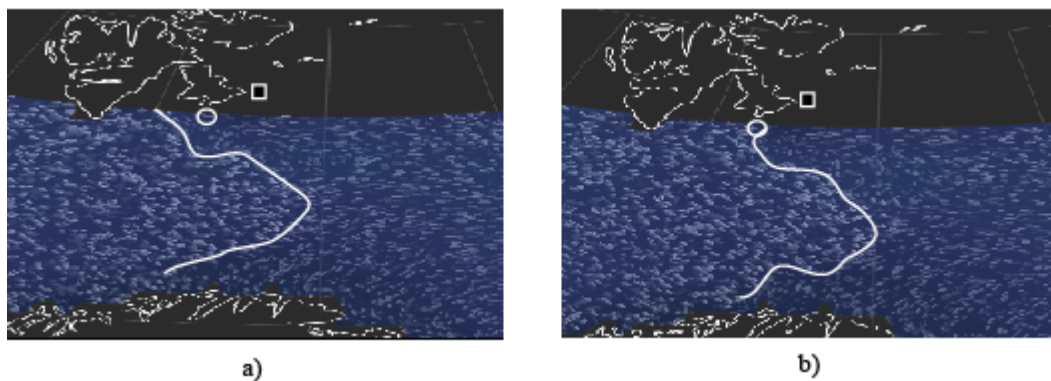


Figure 14. Results from simulations performed by WaveWatch III. Direction of wave propagation are indicated at 22:00, May 01, (a), and 02:00, May 02 (b).

## REFERENCES

1. Collins, C,O., Rogers, W.A., Marchenko, A., Babanin, A.V., 2015. In situ measurements of an energetic wave event in the Arctic marginal ice zone. Geoph. Res. Letters, 42, 6, 1863-1870.
2. Liu, A. K. and E. Mollo-Christensen, 1988. Wave propagation in a solid ice pack, J. Phys. Oceanogr., 18(11), 1702-1712.

3. Marchenko, A.V., Morozov, E.G., Muzylev, S.V., 2013. Measurements of sea-ice flexural stiffness by pressure characteristics of flexural-gravity waves. Annals of Glaciology, 54(64), 51-60.
4. Marchenko, A.V., Gorbatsky, V.V., Turnbull, I.D., 2015. Characteristics of under-ice ocean currents measured during wave propagation events in the Barents Sea. POAC15-00171, Trondheim, Norway.
5. Rabault, J., Sutherland, G., Ward, B., Christensen, K.H., Halsne, T., Jensen, A., 2016. Measurements of Waves in Landfast Ice using Inertial Motion Units. IEEE Transactions on Geoscience and Remote Sensing, 54(11), 6399-6408.
6. Sutherland, G., Rabault, J., 2016. Observation of wave dispersion and attenuation in land fast ice. Journal of Geophysical Research, Oceans, 121, 3, 1984-1997.